Crack Initiation and Propagation during High-Temperature Fatigue of Oxide Dispersion-Strengthened Superalloys

D.M. ELZEY and E. ARZT

The mechanisms of crack initiation and propagation have been investigated in two oxide dispersion-strengthened (ODS) Ni-base superalloys under conditions of symmetric low-cycle fatigue (LCF) and creep-fatigue. The behavior of both ODS alloys is compared with that of conventional alloys of otherwise similar composition. While the improvement in fatigue resistance previously reported for ODS metals and alloys is confirmed by the present study for temperatures below about $0.6T_m$, the potential advantage of dispersion strengthening is not being exploited by the current generation of ODS superalloys at higher temperatures; crack initiation is found to occur prematurely due to the presence of recrystallization defects in the form of fine grains. The mechanism of crack initiation at fine grains is creep-type cavitation on boundaries transverse to the applied stress. Experimental results indicating the influence of temperature, loading frequency, and waveshape on the crack initiation rate are presented and discussed in detail. A qualitative correlation between waveshape and creep-fatigue life is suggested based on the macroscopic inelastic strain rate which is determined by the waveform and limits in turn the rate at which cavity growth can be accommodated.

I. INTRODUCTION

ALLOYS strengthened by a fine, homogeneous dispersion of oxide particles represent a relatively new class of materials intended for critical high-temperature applications, such as gas turbines. Among the important material properties required for such applications are excellent creep strength and corrosion resistance. The superior creep strength of dispersion-strengthened alloys at very high temperatures and relatively low stresses in comparison with dispersion-free alloys has motivated a great deal of study of the creep behavior of these materials.[1,2,3] As a consequence, the mechanisms responsible for the improvement of creep resistance, obtained by introducing a fine dispersion, are now reasonably well understood.[4] Certain applications, such as gas turbine blades and vanes, require, in addition to creep strength, adequate resistance to high- and low-cycle fatigue (HCF and LCF, respectively). The fatigue behavior of dispersion-strengthened alloys is much less well documented, and in particular, the role of the dispersion in determining the high-temperature fatigue strength is only poorly understood. The current study of the high-temperature cyclic behavior of the oxide dispersion-strengthened (ODS) superalloys INCONEL* MA 6000 and MA 754 has been undertaken in order to determine the mechanisms leading to failure under these conditions and to compare the fatigue behavior of modern ODS superalloys with that of conventional high-strength turbine alloys.

Oxide dispersion-strengthened superalloys such as MA 6000 and MA 754 are powder metallurgy materials produced by means of the mechanical alloying (MA) process.[5] Here, elemental and master powders are blended together with the fine dispersoid particles and subsequently milled in a high-energy steel ball attritor. The fully mixed compact is then extruded. A final recrystallization heat treatment is applied in order to obtain the coarse, directional grain structure needed for optimal high-temperature creep resistance.

Prior to the advent of dispersion-strengthened superalloys made possible by the MA process, investigations of the potential of dispersion strengthening were practically limited to elemental metals (Pb, Cu, Al, or Ni), for which the difficulties of introducing the dispersed second phase were surmountable. Perhaps the earliest report of the fatigue behavior of a dispersion-strengthened metal is that due to Martin and Smith[6] for Cu-containing SiO_2 and Al_2O_3 particles. The authors reported an improvement in the room-temperature fatigue strength due to the presence of the hard second-phase particles. Similar results were later obtained for Pb-PbO[7,8] and for Al-Al_2O_3 alloys.[9]

The superior fatigue resistance of dispersion-strengthened metals and alloys is frequently attributed to the increased homogeneity of plastic deformation during cycling.[10-13] This phenomenon, referred to as "slip dispersal," is well documented and arises from the particles acting as obstacles to dislocation motion; dislocation pileups at the particles lead to localized cross slip and the activation of alternative slip planes. While slip dispersal appears to be an effective means of inhibiting crystallographic crack initiation, crack propagation has been found to be negligibly affected by a dispersion.[11,13]

Similarly, recent investigations of ODS superalloys have

*INCONEL MA 6000 and MA 754 are trademarks of Inco Alloys International, Inc., Huntington, WV.

D.M. ELZEY, formerly with Max-Planck-Institut für Metallforschung, is Research Assistant, Department of Materials Science, University of Virginia, Charlottesville, VA 22901. E. ARZT, Professor of Materials Science, is with University of Stuttgart and Max-Planck-Institut für Metallforschung, D-7000 Stuttgart 1, Federal Republic of Germany.

Manuscript submitted July 30, 1990.

demonstrated superior HCF resistance relative to conventional superalloys.[12,14] However, results of LCF testing, most notably at high temperature, have not consistently demonstrated the advantage of dispersion-strengthened alloys.[15] Our present results show clearly that with the increasing importance of creep damage mechanisms at higher temperatures and lower loading frequencies, lifetime may be determined by processes which are less influenced by mechanisms of dispersion strengthening. Instead, we underscore the important role of the grain structure in optimizing fatigue strength in these alloys.

II. EXPERIMENTAL

A. *Materials*

The compositions of INCONEL MA 6000 and MA 754 are shown in Table I. Two conventional (non-dispersion-strengthened) alloys with otherwise comparable chemical compositions were studied for comparison. MA 6000 is strengthened by coherent γ'-precipitate particles [*i.e.*, $Ni_3(Al, Ti)$ with $L1_2$ structure], which are mainly responsible for intermediate temperature strength, and by the dispersion of incoherent oxide particles (~1.1 wt pct Y_2O_3), which impart high-temperature strength (at $T > 900$ °C) (Figure 1). After a secondary recrystallization heat treatment, MA 6000 possesses a grain structure highly elongated in the direction of extrusion (Figure 2). Grain aspect ratios (GAR = ratio of grain length to width) range from 15 to 25 for fully recrystallized macrograins. Table II summarizes some of the microstructural dimensions for MA 6000 as reported in the literature. During recrystallization, the grains of MA 6000 assume a ⟨110⟩ texture in the direction of extrusion. The appearance of a strong texture has also come to be recognized as a characteristic feature of ODS superalloys.[16]

MA 754 consists of an austenitic solid solution of Ni and 20 pct Cr with approximately 1.1 wt pct Y_2O_3 (Table I). The elongated grain structure (GAR > 10) is attained by isothermal annealing. Some physical

Table I. Elemental Composition of Oxide Dispersion-Strengthened Alloys and Their Conventional Counterparts

	MA 6000	IN 738	MA 754	NIMONIC 75
Ni	bal.	bal.	bal.	bal.
Cr	15.5	15.9	20.5	20
Al	4.5	3.5	0.3	0.25
Ti	2.5	3.5	0.35	0.40
W	3.85	2.5	—	—
Mo	2.03	1.6	—	—
Co	—	8.3	—	—
Ta	1.86	1.6	—	—
Fe	—	—	0.13	< 5
Cu	—	—	—	< 0.5
C	0.06	0.09	0.06	0.1
B	0.01	0.01	—	—
Zr	0.16	0.5	—	—
Si	—	—	—	< 1
Y_2O_3	1.08	—	0.5	—

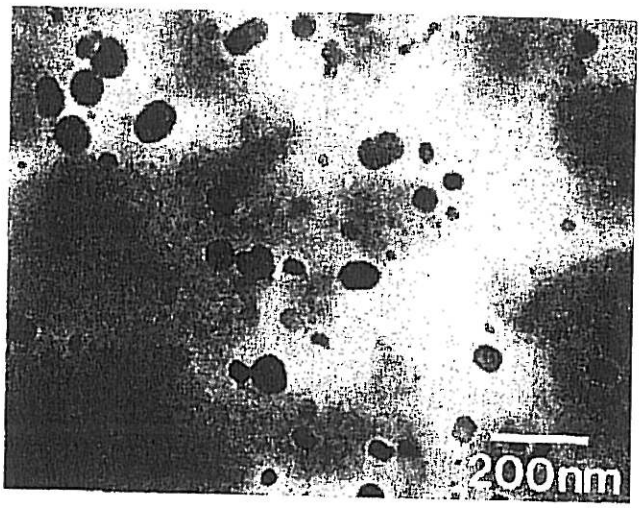

Fig. 1—Y_2O_3 dispersoids in MA 6000 (TEM). The incoherent oxide particles have an average diameter of 33 nm.

dimensions, including grain and dispersoid size, are summarized in Table II. Measurements of the crystallographic texture have revealed a ⟨100⟩ texture in the direction of extrusion, with a preferred ⟨110⟩ orientation in the transverse direction.[17]

Both ODS alloys contain several defect types:[18,19] (a) unrecrystallized zones containing numerous very fine grains of 1- to 5-μm diameter, (b) approximately spherical inclusion particles of approximately 10-μm diameter, which may arise from insufficient powder milling, (c) stringer defects, which appear to be caused by Cr-, Al-, and/or Ti-rich inclusion particles being broken up and then drawn into long strings of much finer particles during extrusion, and finally, (d) fine grains, which appear either singly or in chains of up to perhaps 10 grains and range in size from 10 to 100 μm.

B. *Testing*

Symmetric LCF tests were conducted in the temperature range of 750 °C to 1100 °C and at strain rates of

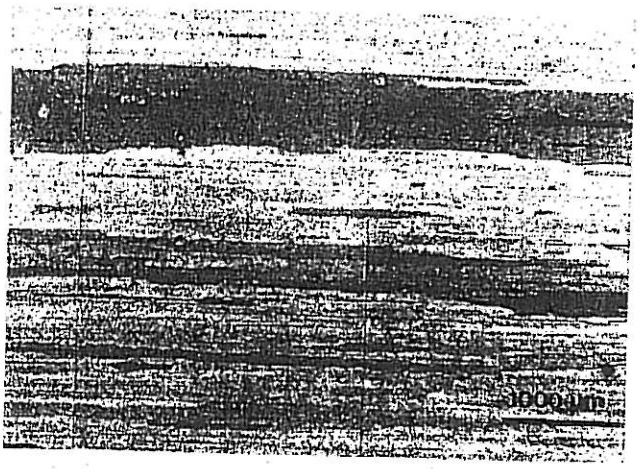

Fig. 2—Highly elongated grain structure in MA 6000. The average grain aspect ratio is about 20 for MA 6000 and 13 for MA 754.

Table II. Microstructural Dimensions of Oxide Dispersion-Strengthened and Conventional Alloys

	Grain Size (mm)	GAR	Particle Diameter (nm)	Particle Spacing (nm)	Texture
MA 6000 (ODS)	5 to 20	20	30	150	⟨110⟩
IN 738	2	1	—	—	—
MA 754 (ODS)	0.6 to 3.2	13	15	130	⟨100⟩
NIMONIC 75	0.1	1	—	—	—

10^{-2} and 10^{-3} s^{-1}. In the case of MA 6000, a number of previous studies have examined the fatigue life as a function of the imposed strain range.[14,20–25] These results have been summarized by Bressers and Arzt.[15] For this reason, the current study of the symmetric LCF behavior of MA 6000 concerns primarily the investigation of crack initiation mechanisms by means of interrupted tests.

The influence of creep deformation and damage on the cyclic behavior may be investigated by applying combinations of very slow and fast strain rates. Such creep-fatigue tests were carried out at 850 °C, 950 °C, and 1050 °C using three different waveforms — "slow-fast" (S-F), tensile hold-time (H-T), and slow symmetric (S-S) (Figure 3). The S-F cycle consists of a slow tensile-going ramp (at 10^{-5} s^{-1}) followed by a rapid compression (at 10^{-2} s^{-1}). The H-T cycle consists of a fast strain reversal (same strain rate as for the compression ramp during S-F tests) with a period of constant total strain in tension. The duration of the hold-times were selected such that the total cyclic period of H-T tests would be the same as that of S-F tests (for a given test strain range). Test conditions and results are summarized for MA 6000 in Table AI and for MA 754 in Table AII of the Appendix.

All tests were conducted in strain control with $R_\varepsilon = -1$ (*i.e.*, fully reversed). Loading of the polished, unnotched, cylindrical test specimens (7 mm diameter with 15 mm gage length) was applied uniaxially in the direction of extrusion. The heating of test samples was accomplished using an induction coil. All tests were conducted in air. For further details, the reader is referred to Elzey.[19]

In addition to tests conducted until rupture of the sample, interrupted tests were carried out, which allowed investigation of the early phases of damage. Such specimens were either broken in tension after cooling in liquid nitrogen or were removed intact. Sections removed from whole or fractured samples, which were then polished and etched, as well as fracture surfaces, were investigated by means of light and scanning electron microscopy (SEM). Some investigations by transmission electron microscopy (TEM) were conducted to gain qualitative information about dislocation arrangements.

In the following, "failure" will be used to indicate the number of cycles at which a 50 pct decrease in the tensile load may be observed, as measured from an extrapolated line of steady softening. Such a definition is possible, since, as a rule, a steady cyclic softening was observed for both ODS alloys under all conditions tested.

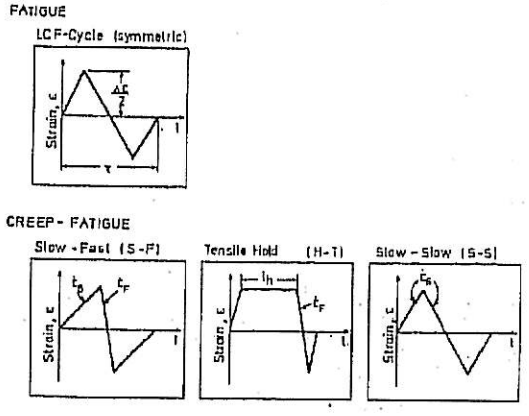

Fig. 3—LCF and creep-fatigue waveforms. Symmetric LCF tests were conducted at frequencies high enough to allow creep deformation to be neglected. All tests were conducted under total strain control.

III. RESULTS

A. *Symmetric High-Temperature Low-Cycle Fatigue (HTLCF)*

1. *Mechanical behavior and lifetime*

The behavior of MA 6000 and MA 754 under conditions of symmetric (triangular) loading and at frequencies sufficiently high to avoid any significant time-dependent effects ($\dot{\varepsilon} \geq 10^{-3}$ s^{-1}) was first investigated. Two tests of MA 6000, one at 850 °C and one at 1050 °C at a strain rate of 10^{-3} s^{-1}, were conducted to failure in order to allow comparison with previous data (Figure 4).

Figure 5 shows the evolution of the peak stress as a function of cycle number for tests on MA 754 at several temperatures and strain amplitudes. This behavior, which was also observed for tests on MA 6000, is characterized by three stages of softening; the first stage exhibits a high rate of softening but is of short duration, followed by a much longer period of steady-state softening. The final stage arises due to macrocrack propagation and signals the imminence of fracture.

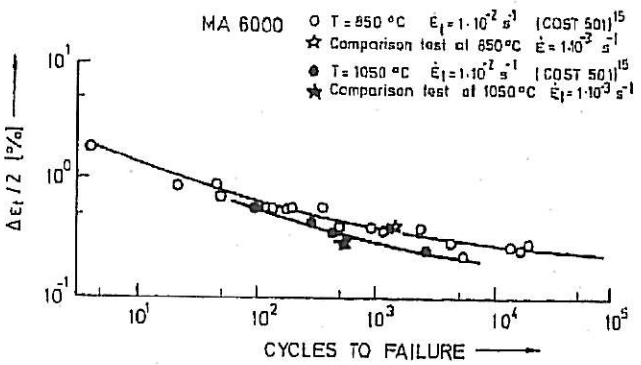

Fig. 4—LCF life of MA 6000 as a function of total strain amplitude at 850 °C and 1050 °C. Two tests (*) conducted to failure for purposes of comparison show good agreement with literature data.

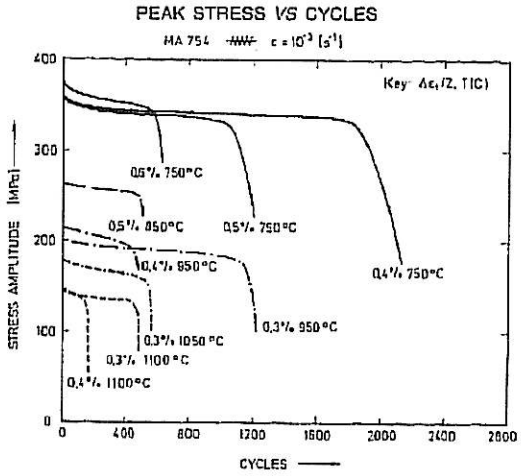

Fig. 5—Both MA 6000 and MA 754 (shown here) exhibit cyclic softening during HTLCF.

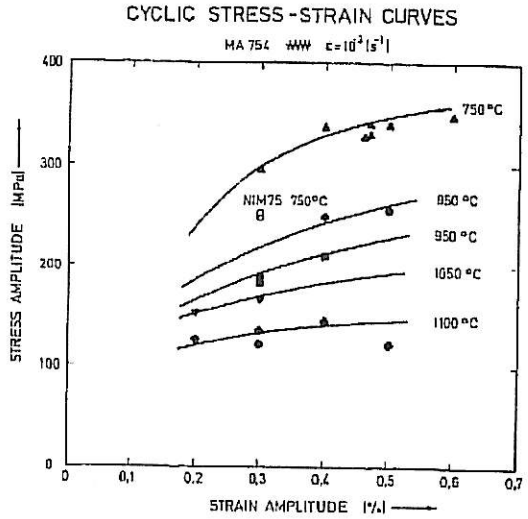

Fig. 7—Cyclic stress-strain curves for MA 754. NIMONIC 75, essentially a non-ODS version of MA 754, has considerably lower cyclic strength.

The LCF life of MA 754 as a function of the applied total strain amplitude and temperature is shown in Figure 6. Data from Nazmy[36] at 850 °C have also been included. Cyclic stress-strain curves (plot of the saturation stress *vs* applied strain amplitude) are given in Figure 7 for MA 754. (Cyclic stress-strain curves for MA 6000 may be found in Bressers and Arzt.[15])

Numerical results of all fatigue tests are summarized in Tables AI and AII of the Appendix.

2. *Metallographic and fractographic results*

Tests to failure of MA 6000 revealed the initiation of surface (or near-surface) cracks as well as occasional internal cracks. This is exemplified by the fracture surface of Figure 8, which shows one internal as well as three surface crack initiation sites.

Polished and etched axial sections revealed that the damage leading to crack initiation occurs frequently at fine grains (defects (d) in Section II–A). Figure 9 illustrates crack initiation at the boundary between two fine grains. Following the initiation of a crack at a fine grain, cracks propagate transgranularly through the surrounding macrograin in a plane perpendicular to the direction of applied stress.

The rough, highly varied fracture surfaces of LCF specimens of MA 754 suggest considerably greater plasticity than in the case of MA 6000 (Figure 10). Examinations of the fracture surfaces reveal no evidence of the propagation of a single macrocrack to failure. Instead, multiple crack initiation occurs with fracture due to coalescence of microcracks.

Figure 11 shows a detail of the fracture surface in Figure 10. It is possible to identify several approximately circular recesses (see arrows), the largest of which is surrounded by a relatively flat area of transgranular crack growth. Such pits are caused by the "pullout" of damaged grains during specimen separation.

During high-temperature low-cycle fatigue (HTLCF)

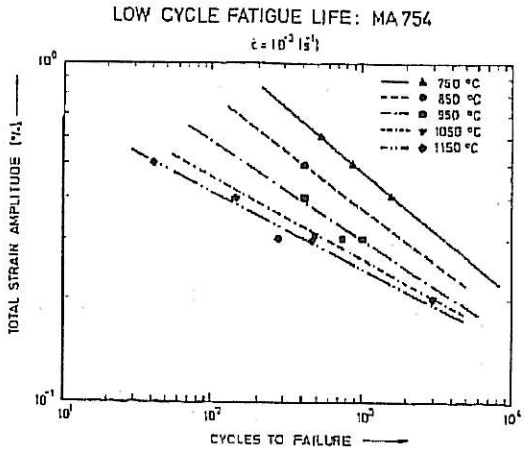

Fig. 6—LCF life of MA 754 as a function of total strain amplitude and temperature.

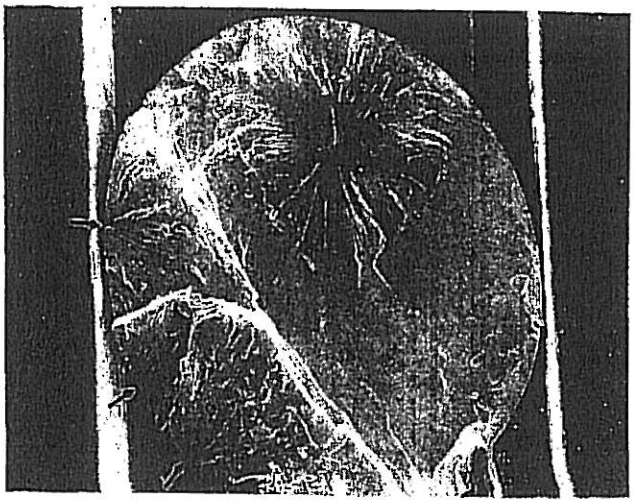

Fig. 8—Fracture surface following symmetric LCF (MA 6000, 850 °C). Four crack initiation sites are visible—three at the sample surface (see arrows) and one in the interior. The smooth region is due to fast fracture (test BB02, Table AI).

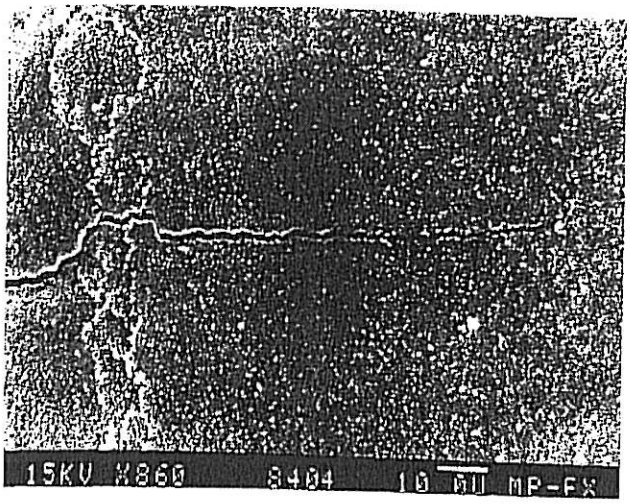

Fig. 9—Crack initiation during LCF (MA 6000, 850 °C) at the boundary between two fine grains. This axial section also shows the subsequent transgranular crack growth through the surrounding macrograin.

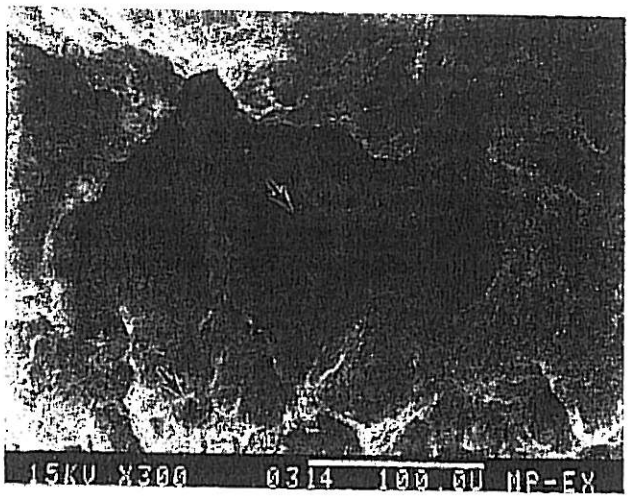

Fig. 11—Internal crack initiation at a fine grain during LCF at 1050 °C (MA 754). A characteristic feature of crack initiation at fine grains is the hole (picture center) left by "pullout" of the damaged fine grain.

of MA 754, cracks may also initiate on or near the surface. This tendency is more apparent at the lower test temperatures (<750 °C to 800 °C). Figure 12 shows a crack which has initiated on a surface-connected grain boundary. This micrograph also illustrates features typical of fatigue crack growth in this alloy, namely, crack branching and crack growth along *longitudinal* grain boundaries.

In order to investigate the influence of the dispersion on the high-temperature fatigue behavior, tests of MA 754, interrupted after 300, 500, and 800 cycles, were compared with identical tests on the dispersion-free alloy NIMONIC* 75. All tests were conducted at a temperature of 750 °C and at a constant inelastic strain range of 0.3 pct. These results revealed that a homogeneous distribution of finely spaced slip bands is visible on the polished surface of the non-ODS alloy, while no slip lines whatever could be identified in MA 754. Crack initiation was observed to occur at surface-connected grain boundaries in NIMONIC 75 under these conditions.

*NIMONIC is a trademark of Inco Alloys International, Inc., Huntington, WV.

3. *Summary of LCF behavior*

The results of our observations of the symmetric LCF behavior of MA 6000 can be summarized in the form of a crack initiation "mechanism map" (Figure 13). Fine grains appear to be responsible for crack initiation under most relevant LCF conditions, especially with increasing temperature.

Crack growth in MA 6000 during HTLCF is either fully transgranular or mixed trans-/intergranular. Figure 14 shows the crack growth mode as a function of

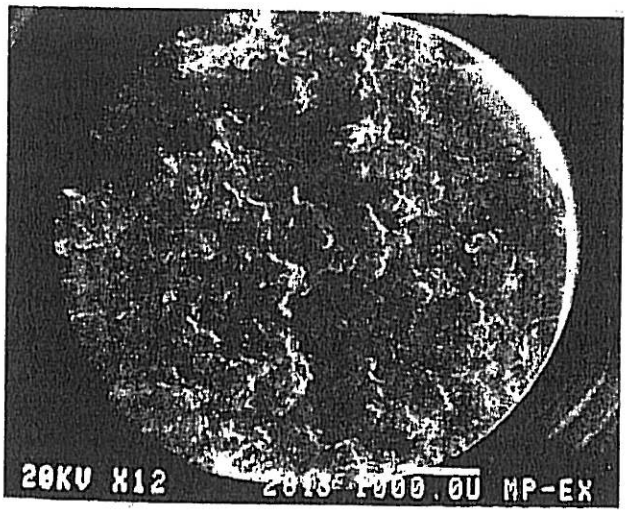

Fig. 10—The roughness of the LCF fracture surface (MA 754, 850 °C) is the result of multiple internal crack initiation and subsequent coalescence, partly along axially oriented macrograin boundaries.

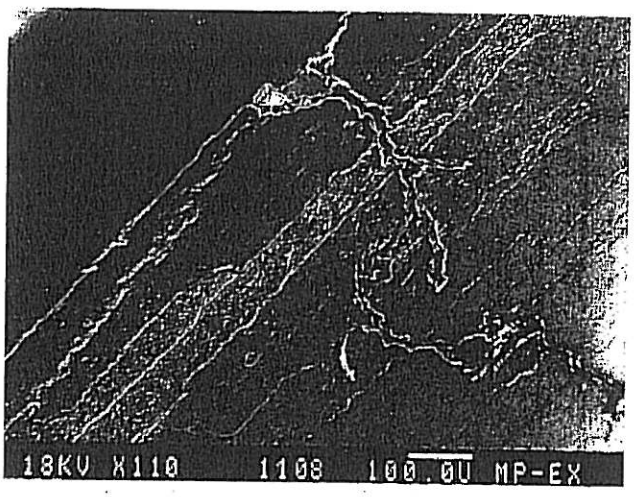

Fig. 12—Crack growth in MA 754 during HTLCF [both the sample surface (dark) and part of an axial section are visible]: the crack has initiated at a surface-connected grain boundary. A tendency for crack branching along planes oriented 45 deg with respect to the stress axis and damage on internal grain boundaries influence the crack growth behavior.

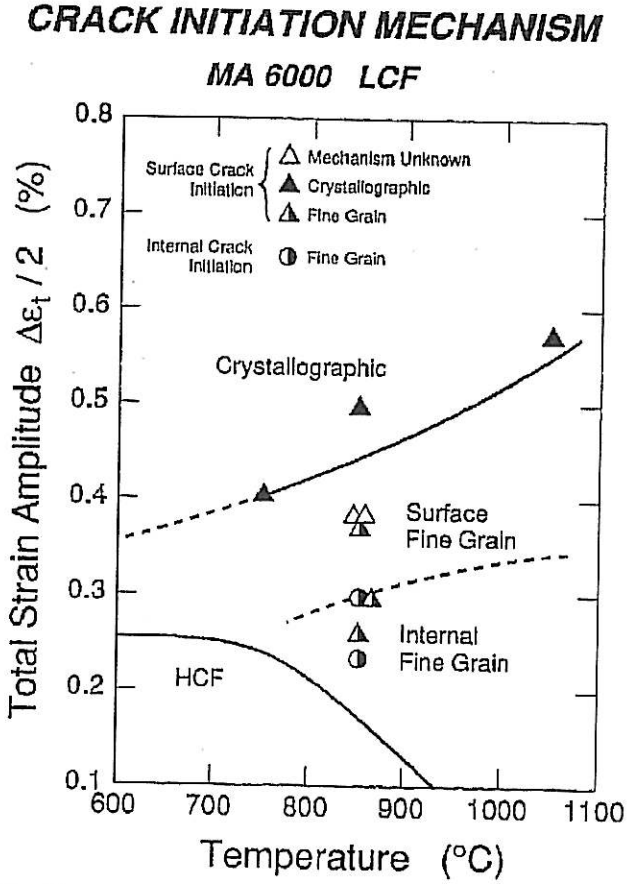

Fig. 13—LCF crack initiation mechanism as a function of temperature and strain amplitude for MA 6000: crack initiation occurs under most conditions due to damage on fine grains; this tendency increases with increasing temperature. At high strain amplitudes, crystallographic damage and slipband cracking become increasingly important.

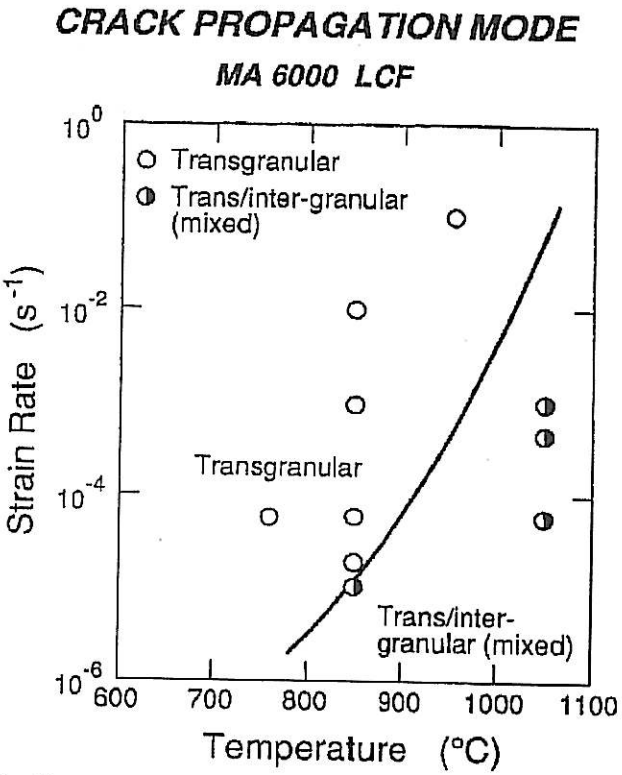

Fig. 14—Crack growth behavior of MA 6000 as a function of strain rate and temperature: fracture is mainly transgranular under all conditions tested; this is attributable to the highly elongated grain structure. Grain boundaries (also those parallel to the stress axis) become increasingly susceptible to fracture with increasing temperature.

strain rate and temperature. Intergranular damage increases with increasing temperature and decreasing strain rate.

Results of HTLCF tests of MA 754 in the temperature range of 750 °C to 1100 °C indicate two crack initiation mechanisms: at lower temperatures (≤800 °C), cracks initiate at surface-connected grain boundaries, while at temperatures greater than about 800 °C, internal crack initiation occurs at fine grains. These observations are summarized in Figure 15.

B. *Creep-Fatigue*

1. *Mechanical behavior and lifetime*

The influence of cycle shape on the fatigue life of MA 6000 may be seen in Figure 16. The S-F cycle leads to a factor of 10 reduction in cyclic lifetime compared with symmetric LCF results (T = 850 °C, $\dot{\varepsilon} = 10^{-2}$). Somewhat less damaging are the S-S cycle (factor of 5 reduction) and the H-T cycle (factor of 4 reduction). Also, S-F results at 1050 °C (Δ) reveal considerably shorter lives than S-F tests at 850 °C.

Figure 17 shows a comparison of the creep-fatigue life of MA 6000 with results of identical tests conducted using IN* 738, a cast, non-ODS alloy. The strengths of the ODS and conventional alloy are comparable.

*IN is a trademark of Inco Alloys International, Inc., Huntington, WV.

Only preliminary investigations of the creep-fatigue behavior of MA 754 were carried out. As for symmetric HTLCF tests, both ODS alloys exhibit cyclic softening during creep-fatigue.

2. *Metallography and fractography*

A typical MA 6000 fracture surface obtained under creep-fatigue conditions is shown in Figure 18. Close examination of the fracture surface reveals that failure has occurred by the initiation, growth, and coalescence of a number of internal cracks. A detail of a single initiation site may be seen in Figure 19, in which the tip of a protruding fine grain is visible. A region of transgranular crack growth (flat, dark area) surrounding the fine grain tip may also be seen.

Conclusive evidence demonstrating that fine grains are indeed responsible for crack initiation during creep-fatigue was obtained by preparing an axial section passing directly through the crack initiation site seen on the fracture surface. The result is shown in Figure 20, in which several fine grains are clearly visible. On the fracture surface, radial lines (river markings) extending outward away from the exposed fine grain tip may be seen. Evidence of cavitation damage is visible on transverse

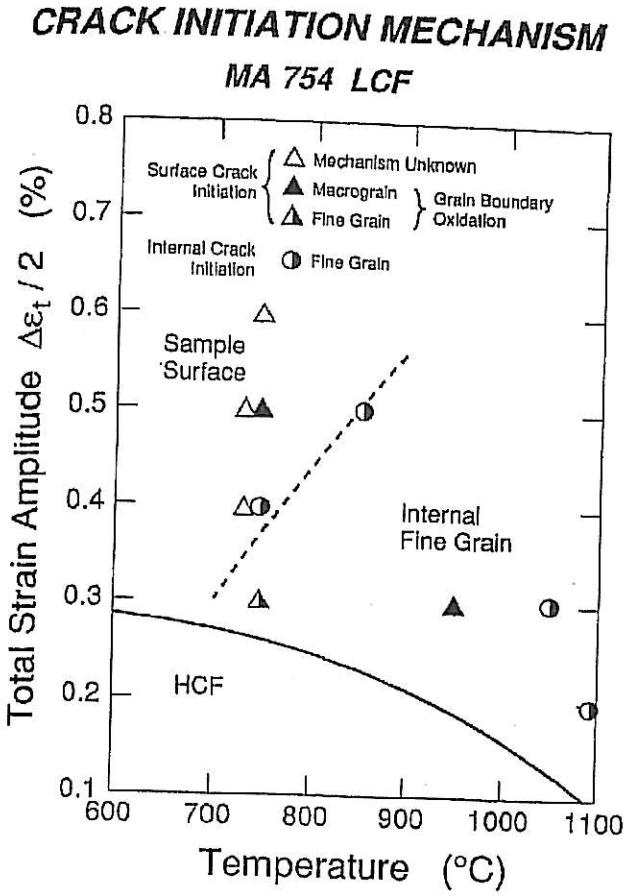

Fig. 15—LCF crack initiation mechanism as a function of temperature and strain amplitude for MA 754: cracks initiate during LCF primarily due to grain-boundary damage—at lower temperatures and higher strain amplitudes on surface-connected boundaries (environmental effect) and by internal damage at fine grains with increasing temperature.

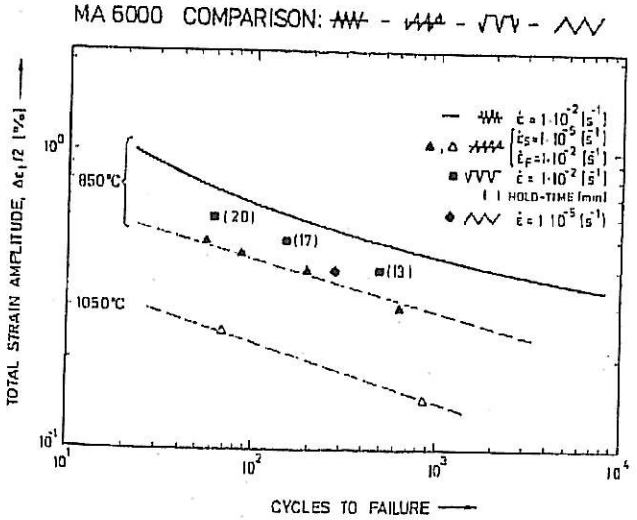

Fig. 16—The influence of creep-fatigue waveform on the cyclic life of MA 6000. All waveforms lead to greatly reduced cyclic life in comparison with symmetric LCF ("fast-fast") data. The S-F cycle leads to a factor of 10 reduction, the S-S cycle to a factor of 5 reduction, and least damaging is the tensile hold-time cycle (factor of 4 reduction).

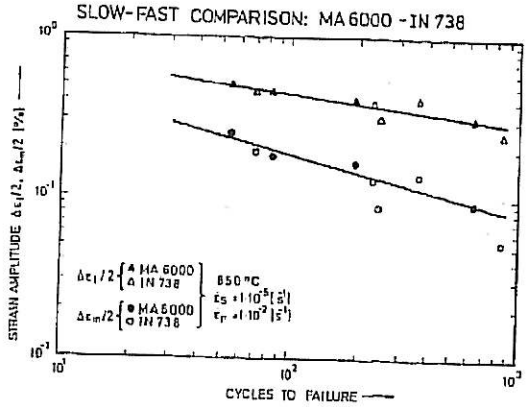

Fig. 17—A comparison of S-F creep-fatigue lifetimes of MA 6000 and IN 738 (data for IN 738 taken from Nazmy);[42] the results for the two alloys are practically identical; only on the basis of plastic strain amplitude does MA 6000 show a slight advantage.

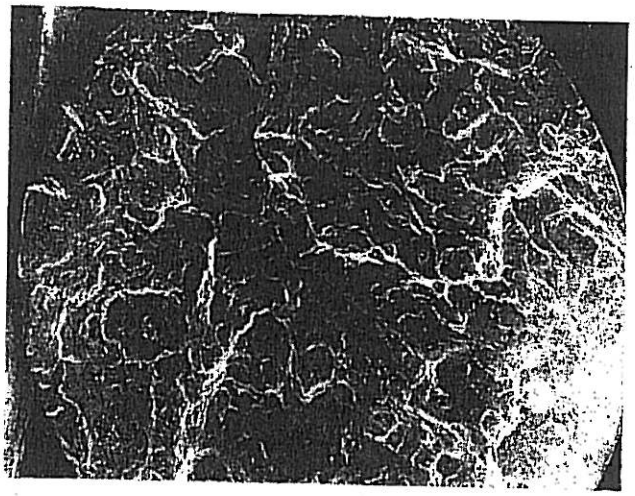

Fig. 18—Fracture surface following slow-fast cycling at 850 °C (MA 6000). More than 25 internal crack initiation sites may be identified (test BD02, Table AI).

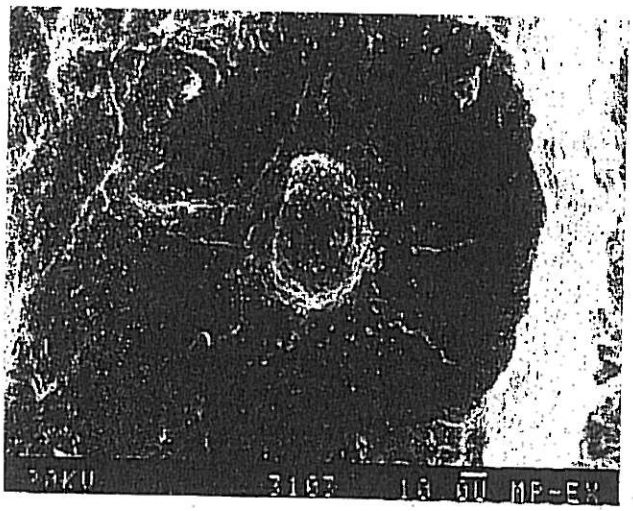

Fig. 19—Crack initiation site as viewed on the fracture surface (S-F, MA 6000). The tip of a fine grain may be seen protruding upward (center). A crack (transgranular and perpendicular to the applied stress) extends radially outward, as evidenced by river markings.

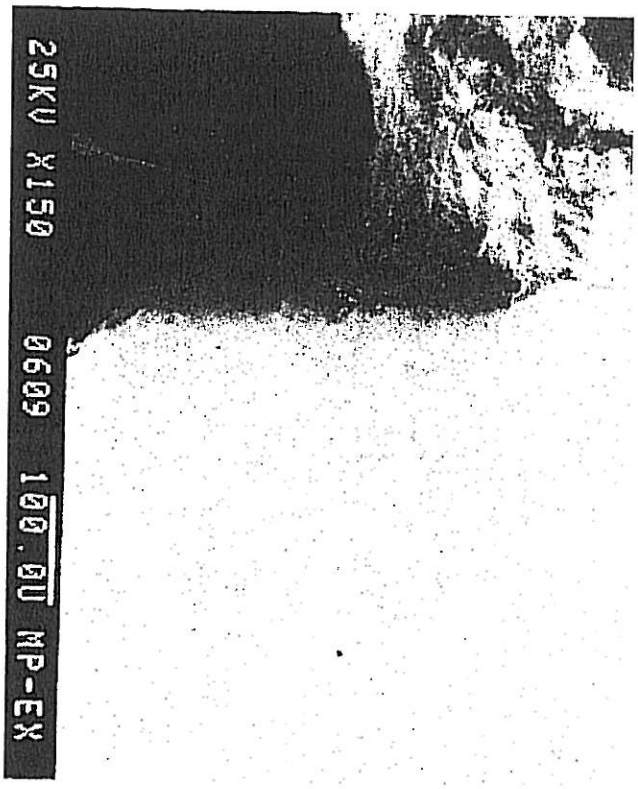

Fig. 20—This micrograph, which has been prepared by cutting an axial section through a crack initiation site, demonstrates clearly that fine grains cause crack initiation. The fracture surface (dark) has been made visible by tilting the sample slightly toward the viewer.

grain boundaries of grain defects (Figure 20). Intergranular cavitation damage is restricted to grain defects; fully recrystallized macrograins did not show evidence of damage under any conditions. Although crack initiation at fine grains has been illustrated by results obtained under S-F conditions (Figures 18 through 20), this mechanism was observed for all creep-fatigue cycle shapes investigated.

In analogy with results of symmetric LCF tests, it was observed that high plastic strain amplitudes lead to an increasing occurrence of crystallographic damage. This results in the introduction of a second crack initiation mechanism, illustrated by Figure 21. Here, a coarse slip band may be seen to intersect a fine grain boundary. Such slip band cracking was observed only in connection with fine-grain boundaries possessing an orientation of between 30 and 60 deg with respect to the direction of applied stress.

Tensile H-T tests revealed the appearance of surface cracks in MA 6000, a feature unique to this type of test. In a few cases, it could be observed that the surface-connected grain boundaries and subsequent intergranular cracks were heavily oxidized. However, the creep-fatigue life of MA 6000 is not determined by the growth of surface cracks, which appear to either grow very slowly or cease growing altogether.

Interrupted creep-fatigue tests showed that damage forms by nucleation and growth of intergranular creep cavities on boundaries perpendicular to the applied stress (Figure 22). The accumulation of cavitation damage leads

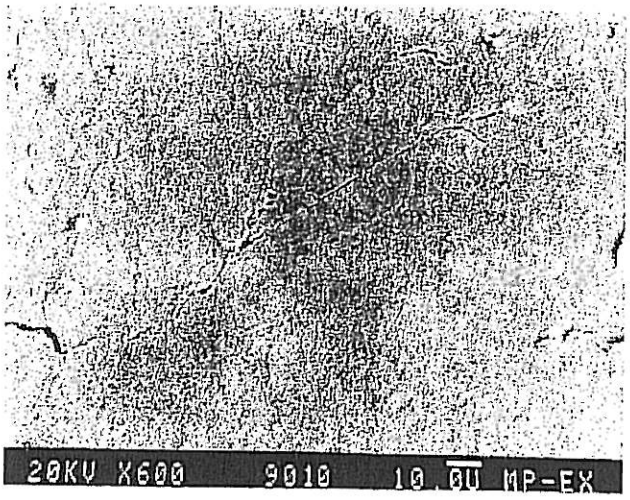

Fig. 21—A second crack initiation mechanism occurs at high plastic strain amplitudes: slip bands interact with grain boundaries to accelerate cavitation damage. Shear strains within the slip band are accommodated by deformation on the grain boundary.

to the formation of a crack which propagates transgranularly into the surrounding macrograin.

Metallographic examination of a series of specimens, all tested under identical conditions but interrupted at progressively larger numbers of cycles (for example at 300, 400, and 500 cycles in the case of an expected life to failure of 700 cycles), provided information concerning the rate of damage accumulation and crack initiation life. In summary of these results, it was found that about two-thirds of the total life under S-F conditions are required before cavitation damage has advanced to the transgranular crack growth stage. Under H-T loading, crack initiation occurs at a smaller proportion of the total cyclic life ($N_i < N_f/2$); however, the crack initiation process is actually slower than under S-F conditions at a given strain amplitude.[19]

A comparison of S-F with symmetric S-S tests (at

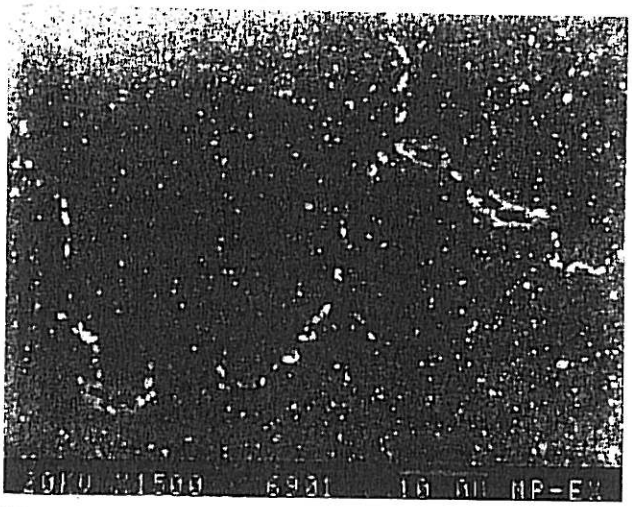

Fig. 22—Cavitation damage on fine grain boundaries during S-F creep-fatigue (MA 6000). Grain boundaries lying perpendicular to the direction of applied stress are most affected.

850 °C, $\Delta\varepsilon = 0.8$ pct, $\dot{\varepsilon} = 10^{-5}$ s^{-1}) interrupted after 155 cycles revealed that while cavitation had already progressed to crack growth in the S-F sample, practically no damage could be observed after slow symmetric loading. Apparently, the symmetric loading leads to at least partial healing of cavities during compression.

Preliminary creep-fatigue tests of MA 754 have confirmed that crack initiation due to cavitation damage at grain defects occurs here as well.

IV. DISCUSSION

A. *Crack Initiation*

The results of this study have shown that grain structure defects are a frequent cause of crack initiation during symmetric HTLCF. This observation is valid for both ODS alloys investigated. Failure is caused by the nucleation and subsequent growth of only a small number of cracks (1 to 4 have been observed), initiating most frequently on or near the sample surface.

Results of creep-fatigue tests of both ODS alloys have demonstrated that there, grain defects are the primary cause of crack initiation. In comparison with symmetric LCF, a much higher density of such cracks is observed under creep-fatigue conditions (a factor of 10 or more in the case of S-F and tensile hold-time tests). Of the three creep-fatigue waveshapes, the symmetric S-S cycle resulted in the lowest density of cracks. This is believed to be the result of cavity sintering during slow compression.

1. *Crack initiation mechanisms*

Although mechanisms of crack initiation during LCF of MA 6000 have been reported by other studies, the harmful influence of grain defects has not been previously identified. Kim and Merrick,[20] who investigated the LCF behavior of MA 6000 at 760 °C, reported the presence of smooth facets on the fracture surface at what was believed to be the crack origin. They concluded that these facets were caused by crystallographic (stage I) crack initiation and growth. The current study has also revealed an influence of coarse crystallographic slip band formation, however, only at relatively high plastic strain amplitudes. In spite of these observations, to the authors' knowledge no clear evidence of slip deformation (SEM or light microscopy showing slip lines, bands, extrusions, *etc.*) during LCF of MA 6000 at low to moderate strain amplitudes has been presented.

Summarizing the results of a number of LCF studies of MA 6000 conducted as part of a cooperative project of the European Community (COST 501 Round I), Bressers and Arzt[15] cited evidence indicating that crack initiation is an environmentally enhanced process; however, no specific mechanism was identified. Other studies cited inclusions as being responsible for the initiation of cracks in MA 6000.[14,24,27] In these studies, the inclusion size was reported to be approximately 70 μm. Since microstructural investigations of as-received material have not revealed inclusions larger than the occasional milling defects, which may reach a diameter of 10 μm or so, it appears likely that fine grains were erroneously identified as inclusion particles (Figure 19). The susceptibility of grain structure defects to crack formation has been reported during stress rupture loading of MA 6000,[18,28] although the effect appears to be much less pronounced than in the case of high-temperature fatigue.

The observation that the transverse boundaries of grain defects are the most frequent sites of crack initiation during symmetric LCF and creep-fatigue indicates an accumulation of damage which is highly localized on these grain boundaries. As mentioned previously, the transverse boundaries of fully recrystallized macrograins are not damaged during fatigue or creep-fatigue. Apparently, fine grains behave differently in response to a given applied stress than do macrograins. The following reason for this observation is suggested: fully recrystallized macrograins exhibit a strong texture and will therefore have little misorientation between each other. The fine grains, however, have arbitrary crystallographic orientation;[29] this leads to high-angle grain boundaries between the fine grain and the macrograin and, therefore, to an increased susceptibility to cavitation. In addition, the fine grains will possess a different elastic modulus in the direction of loading than the textured matrix, which leads to local stress concentrations.

There are other factors which might help to explain the sensitivity of fine-grain boundaries to damage accumulation: (a) a large strength differential between the highly strengthened grain interiors (solid solution, precipitate, and dispersion) and the grain boundaries, (b) the absence of other defects, such as casting pores or large ceramic inclusions, which plague many conventional high-strength alloys, and (c) the suppression of crystallographic crack initiation due to the slip-homogenizing effect of the fine dispersoid particles.

From the similarity of the cavities to creep cavities observed after monotonic loading,[28] we conclude that also during creep-fatigue, creep-type cavities develop which grow by stress-directed diffusion of vacancies from the grain boundary to the void surface. Figure 23 suggests that the mechanism of crack formation during symmetric LCF might be cavitation, too. The phenomenon

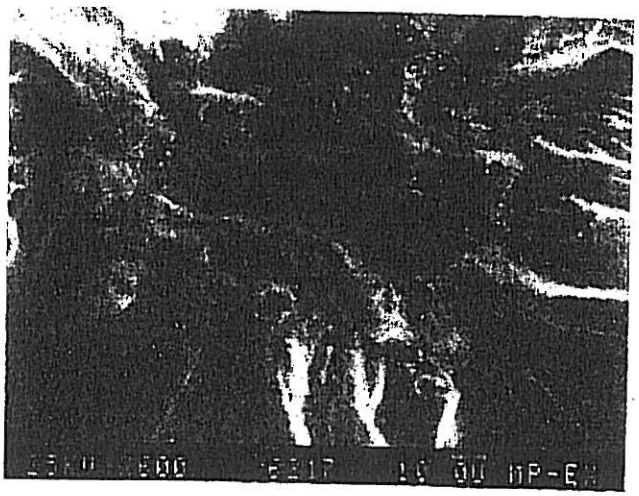

Fig. 23—This detail of an LCF fracture surface shows crack initiation at a fine grain. The large, flat cavities have probably formed by the coalescence of a number of much smaller pores (MA 6000, 850 °C, $N = 5017$ cycles).

of cavity nucleation during symmetric fatigue cycling at frequencies which preclude creep effects is well documented; yet, there exists no generally accepted explanation for it. It is clear, however, that the formation of slip bands and their impingement on hard, second-phase particles is a primary source of cavity nucleation in many engineering alloys (see Gerold[30] for a review of this literature). The grain boundaries in MA 6000 have indeed been shown to contain hard particles, such as larger Y_2O_3 dispersoids and carbonitrides,[31] which could act as cavity nuclei. However, a concentrated study of cavity nucleation and growth during LCF of ODS alloys would be required to confirm this.

An additional mechanism leading to crack initiation has been observed during creep-fatigue at relatively high plastic strain amplitudes ($\Delta\varepsilon_{in} > 0.4$ pct). These results (Section III–B) show that damage on fine grain boundaries may be caused by interaction with slip band cracks (Figure 21) in addition to cavitation. Grain boundaries whose orientation coincides roughly with the direction of slip (generally between about 30 and 60 deg with respect to the direction of applied stress) are susceptible to sliding due to the high applied shear stresses. As sliding occurs, slip deformation within the matrix is accommodated, allowing the development of an actual crack along the slipband. Grain sliding would also be expected to cause stress concentrations within the boundary, leading to enhanced cavity nucleation and growth.[32]

Influence of the dispersion on fatigue deformation behavior

While the non-ODS alloy NIMONIC 75 exhibited a dense array of finely spaced slip bands, slip bands could not be resolved in MA 754 tested under identical conditions. As reported in other experimental studies, in which the fatigue behavior of an ODS alloy has been directly compared with that of a conventional alloy of similar composition, the dispersion inhibits the formation of long, planar slip bands (Leverant and Sullivan[10] for TD-Ni and Ni; Weber and Bomford[12] for MA 753 and NIMONIC 80A).

Obviously particle-dislocation interactions must lead to the activation of alternative slip planes, resulting in a more homogeneous distribution of plastic deformation. Gräf and Hornbogen[33] have convincingly demonstrated that the effect of a finer slip distribution is to delay the nucleation of slipband cracks. The opposite effect can be observed in alloys containing shearable precipitates, where slip tends to become increasingly concentrated as precipitates are sheared. Lütjering[13] has demonstrated both situations for the case of aluminum alloys, for the alloy containing shearable precipitates, the slip distribution becomes extremely inhomogeneous, while the alloy containing hard particles exhibits finer slip and delayed crack initiation. In MA 6000, the effect of the nonshearable dispersoids overrides that of the coherent γ' particles: only at very large strain amplitudes does crystallographic crack initiation occur. MA 754, which does not contain shearable particles, never showed this stage I nucleation.

The positive influence of a fine dispersion on the deformation during fatigue also becomes quite evident when

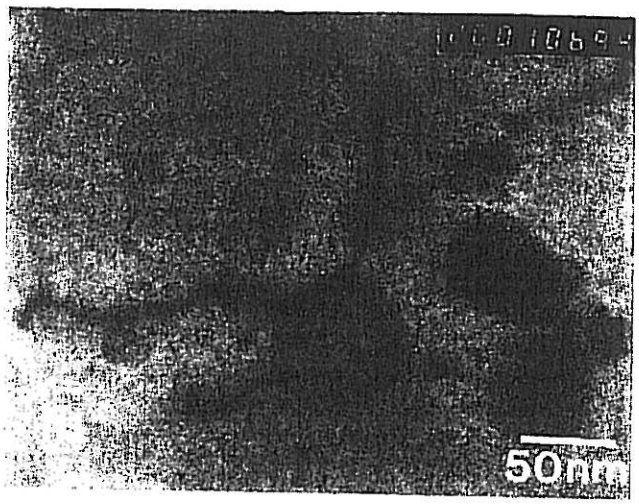

Fig. 24—Typical dislocation structure in fatigued MA 6000 (LCF, 850 °C, $\Delta\varepsilon_t/2 = 0.3$ pct, $\dot{\varepsilon} = 10^{-1}$, $N = 1330$ cycles). Dislocations are frequently pinned by dispersoids.

examining samples by means of TEM. Figure 24 illustrates some features characteristic of ODS alloys subjected to HTLCF: dislocation pinning at dispersoids (see References 31, 34, 4, and 35 for a detailed explanation of this high-temperature strengthening mechanism), generally low dislocation density, and the absence of long-range cell structures. These observations are in agreement with other investigations.[20,14]

2. *Creep-fatigue interaction*

Our metallographic results demonstrate that the initiation of cracks during creep-fatigue occurs almost exclusively by the nucleation and growth of intergranular creep cavities. In contrast to symmetric LCF, cavitation under creep conditions is experimentally well documented,[36] and considerable progress toward a theoretical understanding has been made.[37] Simple models for cyclic lifetime prediction for materials which fail by cavitation during creep-fatigue assume no influence of cyclic straining on cavity nucleation and growth rates. Unfortunately, except for very special circumstances, predictions so arrived at overestimate the number of cycles to failure. A number of possible creep-fatigue interaction mechanisms have been studied, some of which might explain the acceleration of cavitation processes during creep-fatigue. These include cavity nucleation on sliding grain boundaries which contain ledges or hard particles,[32] nucleation due to slip bands impinging on second-phase particles, accelerated cavity growth due to vacancy production during cyclic straining,[38] nucleation of wedge cracks during asymmetric fatigue,[39] and accelerated diffusion due to local residual stresses near second-phase particles.[40,41]

Evidence for a creep-fatigue interaction mechanism leading to accelerated cavity nucleation was found by comparison of cavity densities in MA 6000 following S-F creep-fatigue, with samples crept for roughly the same lifetime and at a stress level approximately equal to the time-averaged stress obtaining during

creep-fatigue; these observations revealed a much higher (roughly a factor of 5) grain-boundary cavity density than for creep.

The most likely explanation for the accelerated cavity nucleation rate during creep-fatigue appears to be the interaction of slip bands (although too short and/or wavy to be directly observable in ODS alloys) with dispersoid particles lying on the grain boundary. Also, the introduction of residual stresses near hard particles could, depending on the waveshape, be expected to influence the rate of cavity nucleation.[40,41,19]

3. *Cycle-shape effects*

Of the cycle shapes employed, slow tension combined with fast compression (S-F) results in the greatest reduction in life as compared to symmetric LCF, followed by S-S and, finally, by tests with tensile hold-times. Nazmy[42] has reported a similar influence of cycle shape on the creep-fatigue life of IN 738. These results were attributed to several phenomena, including multiple surface cracking, the development of mean stresses during cycling, and differences in crack morphology. Samples subjected to H-T tests were especially likely to develop multiple surface cracks. According to the author, a reduction in crack growth rates may occur as cracks approaching one another on different crack growth planes cause load shedding. The present results for MA 6000 also show that surface cracking is much more frequent during H-T testing, probably because of higher stresses at the sample surface during rapid strain reversal. However, in the case of MA 6000, possibly an environmental interaction ("oxide pegging"), rather than crack-crack interactions, is responsible for the relatively slow growth rates of H-T surface cracks.[23,43]

Concerning mean stresses, strain cycles which are unbalanced toward tension lead to compressive mean stresses, while imbalance toward compression (compressive hold-time test, for example) produces positive mean stresses. Mean stress is here defined as $(\sigma_t + \sigma_c)/2$. In the case of MA 6000, mean stresses defined in this way exist from the first cycle onward and change little with cycling. The time-averaged stress (given by the centroid of the area under the stress-time curve for a given cycle) is *positive* for H-T cycles and provides a better parameter for gaging the damage accumulated per cycle[37] and, hence, also for evaluating the effects of waveform on cyclic lifetime.

The fact that, besides IN 738 and MA 6000, a number of very different engineering alloys which are known to fail by intergranular cavitation exhibit the shortest cyclic lifetime when subjected to S-F loading (*e.g.*, Type 304 Stainless Steel,[44] Al-5Mg),[45] suggests a mechanism relatively independent of composition and microstructure. Since the damage mechanism is known to be intergranular cavitation, an explanation for the observed influence of cycle shape should relate directly to cavity nucleation or growth rates. Under conditions of constant stress, the growth rate of cavities is normally controlled by the rate at which material displaced to the grain boundaries can be accommodated.[46] For the case where accommodation by power-law creep of the matrix is assumed, the remote strain rate $\dot{\varepsilon}^{\infty}$, below which cavity growth is constrained, is given by[46] (formulation here according to Riedel)[37]

$$\dot{\varepsilon}_e^{\infty} = \frac{2\pi^2\sqrt{1 + 3/n} \cdot \Omega \cdot \delta D_b \cdot \sigma_e^{\infty}}{q(\omega)\mathrm{k}T\lambda^2 d}$$

where $q(\omega) = -2 \ln \omega - (3 - \omega)(1 - \omega)$

$$\omega = \left(\frac{2R}{\lambda}\right)^2 \qquad [1]$$

where n is the power-law creep exponent, Ω the atomic volume ($1.09 \cdot 10^{-29}$ m^3), δD_b the grain-boundary thickness times the diffusion coefficient, σ_e^{∞} the remote equivalent stress (= axial stress − transverse stress), ω the cavitated area fraction, $q(\omega)$ a shape factor, R the cavity radius, λ the cavity spacing, k Boltzmann's constant, T the absolute temperature, and d the grain diameter.

Using representative values for MA 6000 (*i.e.*, $n = 6$, $\delta D_b = 3.5 \cdot 10^{-23}$ m^3/s, $\sigma_e^{\infty} = 120$ MPa, $q(\omega) \approx 1$, $T = 1123$ K, $\lambda = 2$ μm, $d = 50$ μm), Eq. [1] gives $\dot{\varepsilon}_e^{\infty} = 3.5 \cdot 10^{-7}$. The tensile strain rate used during S-F tests in this study was 10^{-5}, much higher than $\dot{\varepsilon}_e^{\infty}$ calculated from Eq. [1]. This estimate therefore suggests that cavity growth remains fully unconstrained, and the maximum diffusive cavity growth rate is attained. During the tensile hold-time period of an H-T cycle, the remote inelastic strain rate is given by $\dot{\varepsilon}^{\infty} = -1/E \cdot d\sigma/dt$. Initially, $d\sigma/dt$ is high, but relaxation quickly saturates, leading to strain rates lower than 10^{-8} s^{-1}. Therefore, cavitation rates are expected to be much smaller than under S-F loading. In general, the cycle shape will determine the effective macroscopic inelastic strain rate, which, in turn, determines to what extent cavity growth is constrained. A similar influence of the waveshape could well be expected for any material prone to intergranular cavitation during creep-fatigue.

B. *Crack Growth Behavior during Symmetric LCF and Creep-Fatigue*

Fractographic study of crack growth surfaces in MA 6000 following HTLCF at test temperatures lower than 1050 °C reveals little influence of plasticity—the surface, which in most cases lies perpendicular to the applied stress, is practically featureless, with only occasional striations. This generalized picture of the crack growth behavior is in agreement with the low ductility and fracture toughness reported for MA 6000.[43,47] Also, crack branching, which, when significant, tends to lower the crack growth rate (*e.g.*, in IN 738),[42] has not been observed in MA 6000 here. As expected in an alloy with a high grain aspect ratio (GAR > 20), crack growth is confined largely to a transgranular path. At very high temperatures (>1000 °C), preferential weakening of grain boundaries enhances their susceptibility to fracture, leading to mixed trans-/intergranular crack growth. This transition to mixed crack growth at very high temperature may be enhanced by environmental effects but has also been observed for internal cracks having no contact with the environment.

In contrast with MA 6000, cracks growing in MA 754

during symmetric LCF frequently branch and show a pronounced tendency to propagate along planes of maximum shear stress, *i.e.*, at 45 deg with respect to the direction of applied stress (Figure 12). Ham and Wayman[48] observed a similar phenomenon during fatigue of dispersion-strengthened nickel (TD-Ni); fracture occurred in some cases by the propagation of a single shear crack extending through the entire specimen cross section. Identical tests of nickel without the dispersion did not reveal this behavior. It is plausible that a mechanism similar to that of "void sheeting," developed to explain ductile fracture of steels during tensile loading,[49] is responsible—microvoids are nucleated at second-phase particles due to stresses at the particle-matrix interface. Macroscopic shear deformation occurs by necking of the ligaments between voids. It is probable that high-strength alloys with relatively low ductility, such as MA 6000, would not be as susceptible to this type of fracture mechanism as MA 754 or TD-Ni. Ductile alloys without a dispersion of second-phase particles are equally unlikely to exhibit this behavior.

Regarding the influence of cycle shape, it is to be expected that not only the crack initiation rate will be affected, but the crack propagation rate as well. Fatigue crack growth studies of these effects using fracture mechanics-type specimens have not been reported for MA 6000 or MA 754; however, crack growth rate measurements for MA 6000 subjected to a triangular waveshape at various frequencies ranging from 0.01 to 10 Hz have been made at high temperature.[43] These results indicate that time-dependent effects do not become noticeable until the frequency is reduced to about 0.01 Hz and the temperature increased to about 950 °C. Additionally, Martin and Tekin[29] have investigated the effect of a short hold-time at peak load. Introduction of an hold-time at minimum load had no effect on the crack growth rate, while a hold at the maximum stress intensity caused crack growth to stop. This unexpected result was attributed to environmentally induced crack branching. Although crack branching has not been observed for surface cracks created during creep-fatigue of MA 6000 in the present study, this could explain why failure occurs even under these conditions by the growth of internal cracks rather than by the growth of cracks initiating at the sample surface.

At the frequencies employed for creep-fatigue testing during this work ($\nu < 0.003$ Hz), the roles of time-dependent deformation and damage are, in most cases, quite apparent. Figure 25 illustrates this point for a crack initiated at a fine grain during S-F loading at 850 °C. The transverse boundary is fully damaged, and a transgranular crack extends radially into the surrounding macrograin. Precipitate-free zones are visible near the root of the transgranular crack and also within the ligaments separating the cavity growing ahead of the crack tip and the crack itself. The presence of precipitate-free zones indicates the important role of diffusion as a mechanism of cavity growth. While cracks which are relatively short ($\leq$20 μm) appear to propagate by the nucleation and growth of cavities in the matrix ahead of the crack tip, longer cracks exhibit a different behavior; crack tips, in general, are sharper, and cavities are no longer visible directly ahead of the crack.

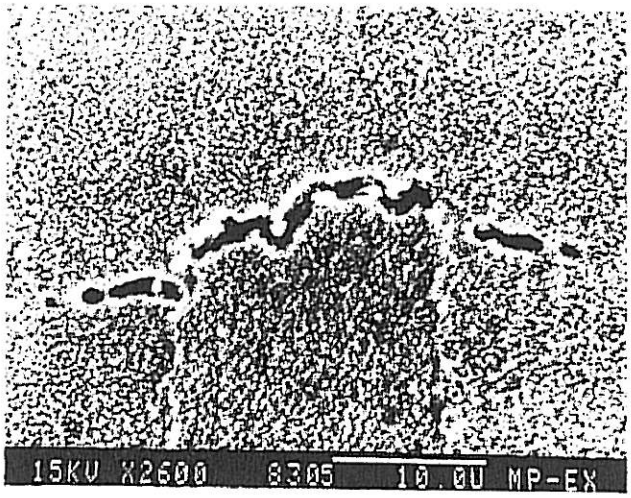

Fig. 25—Short cracks grow by the nucleation and coalescence of pores in the matrix ahead of the crack tip. (S-F test interrupted after 155 cycles).

Some observations concerning the influence of waveform on the crack growth rate may be drawn from an analysis using fracture mechanics-type correlation parameters.[19] The crack geometry, taken as representative of the situation occurring during creep-fatigue of MA 6000, is that of a fully embedded, penny-shaped crack. Since cracks usually initiate by cavitation damage on transverse boundaries of fine grains, the starting crack size is taken to be the average diameter of these fine grains. A comparison of the average crack growth rates during creep-fatigue with literature fatigue crack growth rate (FCGR) data ($0.1 \leq \nu \leq 50$ Hz) demonstrates that creep-fatigue crack growth occurs at stress intensities which are typically at or below the threshold stress-intensity for non-time-dependent fatigue. It is therefore apparent that the crack growth rate during creep-fatigue is greatly accelerated due to the influence of creep deformation and damage mechanisms discussed above.

Only in the case of tensile hold-time tests does the application of an elastic crack growth rate analysis (ΔK) appear to correlate with experimentally determined FCGR. This indicates that crack growth occurs primarily due to the strain reversal ($\dot{\varepsilon} = 10^{-2}\ s^{-1}$) and that the relaxation observed during the period of constant total strain greatly limits the time-dependent growth. During S-F cycling, time-dependent effects are much more important, as reflected by the necessity of including the effects of creep (accomplished by use of the C^* parameter) in order to obtain reasonable agreement with experimental data.

V. CONCLUSIONS

The following conclusions may be drawn from this study:

During high-temperature low-cycle fatigue, cracks initiate most frequently at recrystallization defects in the form of fine grains embedded in the fully recrystallized macrograins. In MA 6000, cracks usually appear on or

near the sample surface. Crack initiation in MA 754 occurs either on the sample surface, which is usually a result of environmental attack of surface-connected grain boundaries, or within the specimen interior, in which case initiation occurs due to the presence of fine grains.

While studies have shown that MA 6000 possesses clearly superior HCF strength relative to its non-ODS counterpart, IN 738, the lifetime under LCF and creep-fatigue of both alloys is comparable. This behavior may be attributed to the increasing effect of time-dependent damage with decreasing loading frequency, to which grain structure defects in ODS superalloys are particularly susceptible.

Crack initiation occurs at fine grains during creep-fatigue regardless of cycle shape; however, the rate of damage leading to crack initiation is very much a function of waveshape. Application of slow-fast cycles leads to the greatest reduction (≈ factor of 10) in cyclic lifetime relative to symmetric LCF results, followed by slow-slow tests (≈ factor of 5 reduction), and lastly, by tensile hold-time tests (≈ factor of 4 reduction).

The observed influence of cycle shape on the creep-fatigue life of alloys (including ODS) subject to intergranular cavitation can be explained qualitatively by considering the effect of waveshape on cavity constraint. Strain rates applied during S-F cycles permit high cavity growth rates (unconstrained), while tensile strain hold-times lead to a high degree of constraint and correspondingly longer lifetimes.

The potential fatigue strength to be attained by the introduction of dispersion strengthening is not being fully exploited by the current generation of ODS superalloys. While the dispersion suppresses the nucleation of crystallographic cracks by inducing a more homogeneous slip distribution, recrystallization defects lead to premature crack initiation. Elimination of these defects should enable substantial improvements in the high-temperature fatigue strength of ODS alloys to be realized.

APPENDIX

Table AI. MA 6000: Numerical Results of Fatigue Experiments

Test No.	Test Type	Temp. (°C)	$\dot{\varepsilon}_t$ (1/s)	$\dot{\varepsilon}_c$ (1/s)	τ^* (s)	$\Delta\varepsilon$ (Pct)	$\Delta\varepsilon_{el}$ (Pct)	$\Delta\varepsilon_{in}$ (Pct)	$\Delta\sigma$ (MPa)	$\Delta\sigma_t/2$ (MPa)	$\Delta\sigma_c/2$ (MPa)	$N_i/2$**	N_i†	N_f
BB01	TRI	1050	10^{-3}	10^{-3}	12	0.6	0.350	0.250	468	221	−247	170	352	505
BB02	TRI	850	10^{-3}	10^{-3}	16	0.8	0.654	0.146	1027	488	−538	650	1330	1555
BX01	TRI	850	10^{-3}	10^{-3}	16	0.8	0.642	0.158	943	458	−485	100	105§	
BX02	TRI	850	10^{-3}	10^{-3}	16	0.8	0.612	0.188	1011	491	−520	100	100§	
BX05	TRI	850	10^{-2}	10^{-2}	1.2	0.6	0.560	0.040	981	462	−519	2000	2028§	
BX08	TRI	850	10^{-2}	10^{-2}	1.2	0.6	0.544	0.056	1022	72	−550	1500	2100§	
BX06	TRI	850	10^{-2}	10^{-2}	1.2	0.6	0.544	0.056	1016	510	−506	3000	3748§	
BX09	TRI	850	10^{-2}	10^{-2}	1.2	0.6	0.550	0.050	955	555	−400	4425	5017§	
BX07	TRI	850	10^{-2}	10^{-2}	1.2	0.6	0.560	0.040	1013	501	−512	8000	8000§	
BB03	S/S	850	10^{-5}	10^{-5}	1600	0.8	0.548	0.252	874	422	−452	45	105§	
BB04	S/S	850	10^{-5}	10^{-5}	1600	0.8	0.528	0.272	876	421	−455	130	270	335
BX04	S/S	850	10^{-5}	10^{-5}	1600	0.8	0.520	0.280	863	421	−442	150	155§	
BD04	S/F	850	10^{-5}	10^{-2}	1001	1.0	0.502	0.498	1030	410	−620	50	55	75
BD03	S/F	850	10^{-5}	10^{-2}	901	0.9	0.540	0.360	1054	429	−625	40	84	105
BD01	S/F	850	10^{-5}	10^{-2}	801	0.8	0.472	0.328	1013	416	−597	95	191	242
BD02	S/F	850	10^{-5}	10^{-2}	601	0.6	0.416	0.184	823	351	−472	305	635	735
BX03	S/F	850	10^{-5}	10^{-2}	801	0.8	0.514	0.286	988	400	−588	100	155§	
BD05	S/F	850	10^{-5}	10^{-2}	601	0.6	0.424	0.176	858	373	−485	250	300§	
BD06	S/F	850	10^{-5}	10^{-2}	601	0.6	0.424	0.176	848	364	−484	200	310§	
BD07	S/F	850	10^{-5}	10^{-2}	601	0.6	0.436	0.164	876	385	−491	420	420§	
BD08	S/F	850	10^{-5}	10^{-2}	601	0.6	0.446	0.154	840	369	−471	400	500§	
BD12	S/F	1050	10^{-5}	10^{-2}	501	0.5	0.270	0.230	458	198	−260	25	50	135
BD11	S/F	1050	10^{-5}	10^{-2}	300	0.3	0.270	0.030	387	180	−207	100	620	832§
BD10	S/F	1050	10^{-5}	10^{-2}	300	0.3	0.260	0.040	370	175	−195	100	143	155‡
BH05	H/T	850	10^{-2}	10^{-2}	1200	1.2	0.632	0.568	1500	626	−874	30	60	67
BH04	H/T	850	10^{-2}	10^{-2}	1000	1.0	0.560	0.440	1190	486	−704	90	148	197
BH01	H/T	850	10^{-2}	10^{-2}	800	0.8	0.492	0.308	1113	437	−676	154	460	512
BH02	H/T	850	10^{-2}	10^{-2}	600	0.6	0.474	0.126	940	340	−600	585	715§	

*Cycle period.
**Cycle at which $\Delta\varepsilon_{el}$, $\Delta\varepsilon_{in}$, $\Delta\sigma$, $\Delta\sigma_t/2$, and $\Delta\sigma_c/2$ were determined.
†Cycle at which the peak tensile stress begins to decrease rapidly.
‡Accuracy of lifetime questionable due to experimental difficulties.
§Test interrupted at given number of cycles.

Table AII. MA 754: Numerical Results of Fatigue Experiments

Test No.	Test Type	Temp. (°C)	$\dot{\varepsilon}_t$ (1/s)	$\dot{\varepsilon}_c$ (1/s)	τ^* (s)	$\Delta\varepsilon$ (Pct)	$\Delta\varepsilon_{el}$ (Pct)	$\Delta\varepsilon_{in}$ (Pct)	$\Delta\sigma$ (MPa)	$\Delta\sigma_t/2$ (MPa)	$\Delta\sigma_c/2$ (MPa)	$N_i/2$**	N_i†	N_f
AB04	TRI	1100	10^{-3}	10^{-3}	20	1.0	0.354	0.646	249	122	−127	30	40	80
AB01	TRI	1100	10^{-3}	10^{-3}	16	0.8	0.376	0.424	292	145	−147	50	142	180
AB02	TRI	1100	10^{-3}	10^{-3}	12	0.6	0.340	0.260	244	122	−122	150	277	340
AB05	TRI	1100	10^{-3}	10^{-3}	12	0.6	0.360	0.240	275	135	−140	230	453	535
AB03	TRI	1100	10^{-3}	10^{-3}	8	0.4	0.334	0.066	256	127	−129	1500	2995	5250
AB08	TRI	1050	10^{-3}	10^{-3}	12	0.6	0.400	0.200	335	166	−169	420	510	680‡
AB09	TRI	1050	10^{-3}	10^{-3}	12	0.6	0.380	0.220	337	167	−170	230	467	635
AB12	TRI	1050	10^{-3}	10^{-3}	8	0.4	0.364	0.036	309	153	−156	1000	8420§	
AB13	TRI	950	10^{-3}	10^{-3}	16	0.8	0.454	0.346	410	210	−200	210	410	605
AB07	TRI	950	10^{-3}	10^{-3}	12	0.6	0.418	0.182	378	182	−195	200	750	1100
AB10	TRI	950	10^{-3}	10^{-3}	12	0.6	0.420	0.180	380	188	−192	500	1000	1370
AB11	TRI	850	10^{-3}	10^{-3}	20	1.0	0.520	0.480	518	255	−263	200	415	565
AB14	TRI	850	10^{-3}	10^{-3}	16	0.8	0.520	0.280	503	249	−254	520	940	1495‡
AB17	TRI	750	10^{-3}	10^{-3}	24	1.2	0.672	0.528	707	348	−359	275	530	700
AB16	TRI	750	10^{-3}	10^{-3}	20	1.0	0.648	0.352	684	338	−345	500	860	1435
AB15	TRI	750	10^{-3}	10^{-3}	16	0.8	0.628	0.172	681	338	−343	750	1550	2515
AB06	TRI	< 760	10^{-3}	10^{-3}	12	0.6	0.566	0.034	605	295	−310	3350	6665	9765
AV01	TRI	750	10^{-3}	10^{-3}	16	0.94	0.632	0.308	683	330	−353	300	300§	
AV02	TRI	750	10^{-3}	10^{-3}	16	0.92	0.610	0.310	659	328	−331	500	500§	
AV03	TRI	750	10^{-3}	10^{-3}	16	0.94	0.632	0.308	688	340	−348	600	800§	
AD01	S/F	950	10^{-5}	10^{-2}	801	0.8	0.216	0.584	181	67	−114	15	20	37‡
AD02	S/F	950	10^{-5}	10^{-2}	601	0.6	0.340	0.260	358	161	−197	40	82	137

*Cycle period.
**Cycle at which $\Delta\varepsilon_{el}$, $\Delta\varepsilon_{in}$, $\Delta\sigma$, $\Delta\sigma_t/2$, and $\Delta\sigma_c/2$ were determined.
†Cycle at which the peak tensile stress begins to decrease rapidly.
‡Accuracy of lifetime questionable due to experimental difficulties.
§Test interrupted at given number of cycles.

ACKNOWLEDGMENTS

The authors wish to express their thanks to C. Elzey for assistance with metallographic/SEM studies. This project was supported by the German BMFT (Project Number O3ZYK1228) and carried out, in its initial phase, within the framework of the European Concerted Action COST 501.

REFERENCES

1. R.W. Lund and W.D. Nix: *Acta Metall.*, 1976, vol. 24, p. 469.
2. J.D. Whittenberger: *Metall. Trans. A*, 1984, vol. 15A, pp. 1753-62.
3. A.H. Clauer and N. Hansen: *Acta Metall.*, 1984, vol. 32, p. 269.
4. E. Arzt: *New Materials by Mechanical Alloying Techniques*, Proc. Deutsche Gesellschaft für Metallkunde Conf., E. Arzt and L. Schultz, eds., DGM Informationsgesellschaft, Oberursel, Federal Republic of Germany, 1989, p. 185; also see Refs. 34 and 35.
5. J.S. Benjamin: *Metall. Trans.*, 1970, vol. 1, pp. 2943-51.
6. J.W. Martin and G.C. Smith: *J. Inst. Met.*, 1955, vol. 83, p. 153.
7. D.H. Roberts, N.A. Ratcliff, and J.E. Hughes: *Powder Metall.*, 1962, vol. 10, p. 132.
8. K.U. Snowden: *J. Mater. Sci.*, 1967, vol. 2, p. 324.
9. J.T. Blucher, P. Knudsen, and N.J. Grant: *Trans. AIME*, 1968, vol. 245, p. 1605.
10. G.R. Leverant and C.P. Sullivan: *Trans. AIME*, 1968, vol. 242, p. 2347.
11. G.R. Leverant and C.P. Sullivan: *Trans. AIME*, 1969, vol. 245, p. 2035.
12. J.H. Weber and M.J. Bomford: *Metall. Trans. A*, 1976, vol. 7A, pp. 435-41.
13. G. Lütjering: Habilitationsschrift, Ruhr Universität, Bochum, Federal Republic of Germany, 1974.
14. W. Hoffelner and R.F. Singer: *Metall. Trans. A*, 1985, vol. 16A, pp. 393-99.
15. J. Bressers and E. Arzt: *High Temperature Alloys for Gas Turbines and Other Applications*, Proc. Conf., W. Betz, R. Brunetaud, D. Coutsouradis, H. Fischmeister, T.B. Gibbons, I. Kvernes, Y. Lindblom, J.B. Marriott, and D.B. Meadowcroft, eds., D. Reidel Publishing Co., Dordrecht, The Netherlands, 1986, p. 1067.
16. J.D. Whittenberger: *Mat. Sci. Eng.*, 1982, vol. 54, p. 81.
17. J.J. Stephens and W.D. Nix: *Metall. Trans. A*, 1985, vol. 16A, pp. 1307-24.
18. H. Zeizinger: Ph.D. Dissertation, University of Stuttgart, Stuttgart, Federal Republic of Germany, 1986; in *Fortschr.-Ber. VDI* (in German), 1987, ser. 5, vol. 121.
19. D.M. Elzey: Ph.D. Dissertation, University of Stuttgart, Stuttgart, Federal Republic of Germany, 1989; in *Fortschr.-Ber. VDI* (in German), 1989, ser. 5, vol. 175.
20. Y.G. Kim and H.F. Merrick: *Superalloys 1980*, Proc. Conf., J.K. Tien, ed., ASM, Metals Park, OH, 1980, p. 551.
21. R.G. Wing: *Frontiers of High Temperature Materials II*, Proc. Conf., J.S. Benjamin and R.C. Benn, eds., Inco Alloys International, Huntington, WV, 1983, p. 287.
22. R.L. Dreshfield: *Frontiers of High Temperature Materials II*, Proc. Conf., J.S. Benjamin and R.C. Benn, eds., Inco Alloys International, Huntington, WV, 1983, p. 235.
23. J.W. Martin and A. Tekin: *High Temperature Alloys for Gas Turbines and Other Applications*, Proc. Conf., W. Betz, R. Brunetaud, D. Coutsouradis, H. Fischmeister, T.B. Gibbons, I. Kvernes, Y. Lindblom, J.B. Marriott, and D.B. Meadowcroft, eds., D. Reidel Publishing Co., Dordrecht, The Netherlands, 1986, p. 1057.
24. A.J. Huis in't Veld, P.M. Bronsveld, and J. Th.M. DeHosson: *High Temperature Alloys for Gas Turbines and Other Applications*, Proc. Conf., W. Betz, R. Brunetaud, D. Coutsouradis, H. Fischmeister, T.B. Gibbons, I. Kvernes, Y. Lindblom, J.B. Marriott, and D.B. Meadowcroft, eds., D. Reidel Publishing Co., Dordrecht, The Netherlands, 1986, p. 1049.
25. A. Hynnä, V.-T. Kuokkala, T. Lepistö, T. Mäntylä, and

P. Kettunen: *High Temperature Alloys for Gas Turbines and Other Applications*, Proc. Conf., W. Betz, R. Brunetaud, D. Coutsouradis, H. Fischmeister, T.B. Gibbons, I. Kvernes, Y. Lindblom, J.B. Marriott, and D.B. Meadowcroft, eds., D. Reidel Publishing Co., Dordrecht, The Netherlands, 1986, p. 1091.
26. M.Y. Nazmy: in *Low Cycle Fatigue*, ASTM STP 942, Solomon, ed., ASTM, Philadelphia, PA, 1988, p. 385.
27. A.J. Huis in't Veld, P.M. Bronsveld, J.Th.M. DeHosson, and J. Bressers: *High Temperature Alloys, Their Exploitable Potential*, Proc. Conf., J.B. Marriott, M. Merz, J. Nihoul, and J. Ward, eds., Elsevier Publishing, London, 1987, p. 19.
28. H. Zeizinger and E. Arzt: *Z. Metallkd.*, 1988, vol. 79 (12), p. 774.
29. J.W. Martin and A. Tekin: Final Report, Project UK 2, COST 501, Department of Metallurgy and Science of Materials, University of Oxford, Oxford, United Kingdom, 1987.
30. V. Gerold: in *Ermuedungsverhalten Metallischer Werkstoffe*, Symp. Proc., D. Munz, ed., DGM Informationsgesellschaft, Oberursel, Federal Republic of Germany, 1984, p. 441.
31. J. Schröder: Ph.D. Dissertation, University of Stuttgart, Stuttgart, Federal Republic of Germany, 1987; *Fortschr.-Ber. VDI* (in German), 1987, ser. 5, vol. 131.
32. R. Raj: *Acta Metall.*, 1978, vol. 26, p. 995.
33. M. Gräf and E. Hornbogen: *Scripta Metall.*, 1978, vol. 12, p. 147.
34. E. Arzt and J. Rösler: *Acta Metall.*, 1988, vol. 36, p. 1053.
35. J. Rösler and E. Arzt: *Acta Metall.*, 1990, vol. 38, p. 671.
36. A.J. Perry: *J. Mater. Sci.*, 1974, vol. 9, p. 1016.
37. H. Riedel: *Fracture at High Temperatures*, Springer-Verlag, Berlin, 1987, pp. 175, and 247-60.
38. Y. Ishida and D. McLean: *Met. Sci. J.*, 1967, vol. 1, p. 171.
39. B.K. Min and R. Raj: in *Fatigue Mechanisms*, ASTM STP 675, J.T. Fong, ed., ASTM, Philadelphia, PA, 1979, p. 569.
40. K. Shiozawa and J.R. Weertman: *Acta Metall.*, 1983, vol. 31, p. 993.
41. B. Kempf: Ph.D. Dissertation, University of Stuttgart, Stuttgart, Federal Republic of Germany, 1987.
42. M.Y. Nazmy: *Metall. Trans. A*, 1983, vol. 14A, pp. 449-61.
43. F. Gabrielli and G. Vimercati: Progress Report, Project I 8, COST 501, Inst per la Tecnologia dei Mat Metallici non Tradizionale del C.N.R., Italy, 1985.
44. S. Majumdar and P.S. Maiya: *Can. Metall. Q.*, 1979, vol. 18, p. 57.
45. S. Baik and R. Raj: *Metall. Trans. A*, 1982, vol. 13A, pp. 1215-21.
46. B.F. Dyson: *Met. Sci.*, 1976, vol. 10, p. 349.
47. T.P. Gabb and R.L. Dreshfield: in *Superalloys II*, C.T. Sims, M.S. Stoloff, and W.C. Hagel, eds., J. Wiley and Sons, New York, 1987, pp. 584 and 594.
48. R.K. Ham and M.L. Wayman: *Trans. AIME*, 1967, vol. 239, p. 721.
49. H.C. Rogers: *Trans. TMS-AIME*, 1960, vol. 218, p. 498.